

# A COUPLED THERMOMECHANICAL COHESIVE ZONE MODEL FOR INTERFACE CRACK GROWTH IN THERMAL PROTECTION SYSTEMS

Ashwin Hattiangadi and Thomas Siegmund  
School of Mechanical Engineering, Purdue University, West Lafayette, IN, 47907

## ABSTRACT

A numerical framework for the coupled thermomechanical analyses of structures with growing cracks is outlined. Using a thermomechanical cohesive zone model (TM-CZM) load transfer behavior is coupled to heat conduction across the interface and the interface crack. Non-linear effects arise due to the coupling between the mechanical and thermal problem including the conductance-separation response between crack faces as well as the temperature dependence of the material constants of the TM-CZM. A study of interface delamination in an oxidation protection coating on a composite material substrate under transient thermal loading is presented. The coupling between the thermal and mechanical analyses is demonstrated to affect the crack initiation and growth behavior. The presence of a gas in the crack interface delays crack initiation, while thermal degradation of interface strength accelerates crack growth.

## 1 INTRODUCTION

Previous investigations of the thermo-mechanical behavior of structures containing interface cracks considered steady state thermal conditions [1] for either a perfect interface, or insulated cracks [2-4]. Of recent interest in this context are high-temperature coatings on metal substrates [5-7]. The influence of crack heat flux was found to affect the crack behavior significantly as the interface thermal resistance varied [8]. Significant dependence of the energy release rate on the assumed crack conductance was predicted [9]. However, a coupled thermo-mechanical analysis accounting for crack growth and the resulting changes in heat flux crack has not been conducted.

In this study a formulation is presented that introduces a description of the interface and crack conductance together into the crack growth problem. The coupling between the mechanical and thermal analysis results in a non-linear response. The thermomechanical coupling compliments the mechanical and thermal specimen response with a conduction-separation response and accounts for the temperature-dependent strength degradation of the interface.

The mechanical behavior of cracked specimen is modeled using a cohesive zone model (CZM) [10-12]. The CZM uses a triangular traction-separation law [13] which is modified to include the temperature dependence of the cohesive strength. The traction-separation behavior uses an internal residual property variable that determines the extent of damage caused by material separation. By incorporating temperature dependence, the interfacial strength and therefore the tractions decrease as the applied thermal load increases. The description of thermal transport includes a formulation accounting for the breakdown of interface conductance with increase in material separation. The current state of interface failure, the presence of a gas entrapped in the crack as well as radiative heat transfer determines the cohesive zone conductance. Finally, a thermal contact conductance model is introduced to describe heat transfer across crack faces in contact. The thermomechanical (TM)-CZM is implemented into the finite element code. The implementation bears some resemblance to the thermomechanical contact formulations and hydrogen diffusion through a particle matrix interface model [14-15].

The TM-CZM is applied in the study of interface crack growth initiation and growth in a thermal protection system (TPS) under transient thermal loading. TPS consists of an oxidation

protection coating (SiC) on a carbon-carbon (C-C) composite substrate. Under thermal loads, in corrosive environments and due to the thermal expansion mismatch between coating and substrate, surface cracks are commonly formed in the coating, later promoting the formation of interface defects, and the subsequent delamination growth [16-17].

## 2 MODEL DEFINITION

### 2.1 Formulation

For the solution of the coupled thermomechanical problem of a solid containing a growing interface crack, both the mechanical equilibrium and the energy balance must be fulfilled. In the present approach an interface and the corresponding interface crack are represented as a cohesive zone. In the mechanical equilibrium equation the CZ contribution is given by the cohesive surface tractions,  $\mathbf{T}_{CZ}$ , and the displacement jump across the cohesive surface,  $\Delta$ , along the internal cohesive surface. In the energy balance equation, the contribution of the CZ on the internal surface are described by the product of the cohesive zone heat flux,  $q_{CZ}$ , and the temperature jump across the cohesive surface,  $\Delta\theta$ , [18].

The tangent stiffness matrix,  $\mathbf{K}_{CZ}$ , for the cohesive zone element formulation includes a mechanical part,  $\mathbf{K}_m$ , in terms of the derivatives of tractions with respect to the displacement jumps, and a thermal part,  $K_{th}$ , in terms of the cohesive zone conductance and its temperature dependence, a mechanical-thermal coupling part,  $\mathbf{K}_{mt}$ , representing the temperature dependence of the traction-separation response, and a thermal-mechanical coupling part,  $\mathbf{K}_{tm}$ , accounting for the dependence of the cohesive zone conductance on the displacement jump:

$$\mathbf{K}_{CZ} = \begin{bmatrix} \mathbf{K}_m\{2 \times 2\} & \mathbf{K}_{mt}\{2 \times 1\} \\ \mathbf{K}_{tm}\{1 \times 2\} & K_{th}\{1 \times 1\} \end{bmatrix}_{\{3 \times 3\}} \quad (1)$$

The numerical implementation of the TM-CZM uses cohesive zone elements with linear interpolation functions for the displacement jumps, and nodal values for temperature jumps across the crack. The TM-CZ element was implemented into the finite element program ABAQUS v6.3.1 through the UEL capability.

### 2.2 Load Transfer

The traction-separation response for the interface is described by use of a quasi-linear relationship between separation and traction. It includes an internal residual property variable,  $s$ , which enforces irreversibility in the fracture process. The normal and tangential tractions,  $T_n$  and  $T_t$ , are given in dependence of the displacement jumps across the crack,  $\Delta_n$  and  $\Delta_t$ , by:

$$T_n = \frac{s}{1-s} \frac{\Delta_n}{\delta_n} \sigma_{\max}(\theta_i) \quad \text{and} \quad T_t = \frac{s}{1-s} \frac{\Delta_t}{\delta_t} \tau_{\max}(\theta_i) \quad \text{if } s > 0 \quad (2)$$

with the normal and shear strengths,  $\sigma_{\max}$  and  $\tau_{\max}$ , as functions of the average local interface temperature,  $\theta_i = (\theta_+ + \theta_-)/2$ . The residual property variable,  $s$ , is related to a measure of the normalized displacement jumps and is assigned an initial value of  $s_{ini}$ .

$$s = \min[s_{ini}, \max(0, 1 - \lambda)] \quad \text{with} \quad \lambda = \sqrt{\left(\frac{\Delta_n}{\delta_n}\right)^2 + \left(\frac{\Delta_t}{\delta_t}\right)^2} \quad (3)$$

Choosing  $s_{ini}$  close to unity allows one to construct a traction-separation response with high initial stiffness. This aspect is important to obtain accurate local solutions for both load transfer as well as heat transfer at the crack tip.

Contact interaction is specified along the cohesive zone such that interpenetration of crack faces is prohibited. A linear relationship between contact pressure,  $T_{n,c}$ , and the overclosure is used:  $T_{n,c} = K_c \Delta_n$ . The contact stiffness,  $K_c$ , is assumed to be equal to the initial stiffness of the traction-separation law, Eq. 2.

### 2.3 Heat Transfer

The cohesive zone heat flux,  $q_{CZ}$ , is a product of the temperature jump across the crack,  $\Delta\theta$ , and the cohesive zone conductance,  $h_{CZ}$ . In developing the thermal part of the TM-CZM 1-D heat transfer is considered and described by an irreversible thermal resistor model.

#### 2.3.1 Interface Conductance

The interface conductance model considered in the present study includes contributions from heat transfer across bonded solid-solid parts of the interface, described by the initial interface conductance  $h_{i,ini}$ , as well as contributions of gas present in pores located at the interface. As damage incurs the interface conductance is given by the sum of the initial interface conductance and a contribution of the gas conductance:

$$h_{CZ} = h_i = h_{i,ini}s + \left[ k_{g,0} + C_g \theta_i \right] \frac{(1-s)}{\eta} \quad s < s_{ini} \quad (4)$$

where  $\eta = \delta_n/3$  for  $\Delta_n < \delta_n/3$  and  $\eta = \Delta_n$  for  $\Delta_n > \delta_n/3$ . The conduction through the gas is dependent on the temperature dependent thermal conductivity,  $k_g = k_{g,0} + C_g(\theta_i)$ .

#### 2.3.2 Crack Conductance

When  $s=0$ , a crack has been formed. The roughness of the crack surface is characterized by  $\omega$ . For an open crack the crack conductance depends on conduction through the gas present in the crack and radiation across the crack faces. The gas conductance is a function of the displacement jump across the crack given by  $k_g/\Delta_n$  for  $\Delta_n > 2\omega$ . For displacement jumps  $0 < \Delta_n \leq 2\omega$  the presence of asperities on the crack faces limits the gas conductance to a maximum value of  $k_g/(2\omega)$ . In contact,  $\Delta_n \leq 0$ , the cohesive zone conductance depends on the combination of contact conductance, [19], and the asperity limited gas conductance:

$$\frac{1}{h_{CZ}} = \frac{1}{1.55} \left[ \frac{\omega}{k_{eq} \tan \vartheta} \right] \left[ \frac{E_{eq} \tan \vartheta}{\sqrt{2} T_{n,c}} \right]^{0.94} + 2\omega \left[ k_g + C_g \theta_i \right]^{-1} \quad (5)$$

The effective elastic modulus and the effective conductivity of the material combination of coating and substrate are given by  $1/E_{eq} = (1-\nu_c^2)/E_c + (1-\nu_s^2)/E_s$  and  $1/k_{eq} = 1/k_c + 1/k_s$  where  $E_c$ ,  $\nu_c$ ,  $k_c$  and  $E_s$ ,  $\nu_s$ ,  $k_s$  are Young's modulus, Poisson's ratio and conductivity for the coating and substrate, respectively. Surface roughness,  $\omega$ , and asperity slope values,  $\vartheta$ , are connected by  $\tan \vartheta = \omega^{0.4}$ .

### 2.3 Model Geometry, Loading and Boundary Conditions

Numerical studies of transient thermal loading are carried out for a carbon-carbon (C-C) composite laminate of thickness  $t_s=5$  mm, with an oxidation protection SiC coating of thickness  $t_c=1$  mm on both sides of the laminate. The laminate length is  $2L=50$  mm. At its center the laminate possesses an edge-type crack of initial length of  $a/L=1/3$ . The crack is located at the interface between the C-C laminate and the SiC coating at the heat flux exposed surface of the laminate. Temperature dependent properties for the orthotropic C-C composite laminate and the isotropic SiC coating are assumed. At 300 K  $E=415$  GPa,  $\nu=0.16$ ,  $k=114$  W/(mK),  $\alpha=1.1 \times 10^{-6}/K$ ,

$c_p=715$  J/(kgK) for SiC and  $E_T=6$  GPa,  $E_L=17$  GPa,  $G_T=2.7$  GPa,  $G_L=2.7$  GPa,  $\nu_T=0.3$ ,  $\nu_L=0.13$ ,  $k_T=3.9$  W/(mK),  $k_L=42$  W/(mK),  $\alpha_L=2 \times 10^{-6}/K$ ,  $\alpha_T=0.5 \times 10^{-6}/K$ ,  $c_p=720$  J/(kgK). The mechanical cohesive zone parameters used are  $\sigma_{max}=\tau_{max}=30$  MPa for the simulations with temperature independent CZ parameters, and  $\sigma_{max}=\tau_{max}=90 - 0.0925(\theta_i)$  for the temperature dependent cases, as well as  $\delta_i=\delta_f=5$   $\mu$ m and  $s_{ini}=0.85$ . The thermal cohesive zone parameters used are  $h_{ini}=0.25$  MW/(m<sup>2</sup>K), such that the interface initially poses nearly no resistance to heat transfer,  $\omega=1$   $\mu$ m, and a conductivity of air as 0.032 W/(mK) at 300 K and 0.1 W/(mK) at 1500 K.

Simulations are performed for a traction free laminate. An initial temperature of  $\theta_0=300$  K is assume. The thermal load consists of a prescribed linearly increasing heat flux of rate  $\dot{q}=0.2$  MW/m<sup>2</sup>s. The thermal boundary conditions assume radiative cooling ( $\epsilon=0.7$ ,  $\theta_\infty=300$  K) at the heated surface, convective cooling ( $h=4 \times 10^4$  W/m<sup>2</sup>,  $\theta_\infty=300$  K) at the opposite surface and insulated sides of the laminate. Due to symmetry a half model is considered with the symmetry conditions  $u_y[(x=0), (y=0)]=0$ . Transient coupled temperature-displacement solutions under plane strain conditions are computed. Continuum elements used in the FE model are 4-noded temperature-displacement elements. TM-CZ elements are placed along the entire interface as well as along the initial crack.

#### 4 RESULTS

As the applied heat flux increases stresses are generated due to the mismatch in properties between coating and substrate as well as due to the inhomogeneous temperature distribution resulting from the temperature gradient across the specimen and the thermal disturbance induced by the presence of the initial crack. Stresses finally rise to levels such that the crack starts to grow. Consequently, the thermal conditions in the sample are changed. Figure 1(a) depicts contour plots of the computed transverse heat flux component at times 4.75, 5, 6, and 7s for the case of a temperature independent cohesive strength and vacuum conditions. Initially, heat flux is inhibited only across the center portion of the laminate. However, as the crack length increases, the specimen becomes insulating over a most of its length. In the end heat flux is highly concentrated at the crack tip and over the small remaining ligaments. Corresponding contour plots of the temperature distributions are shown in Figure 1(a). Initially, a nearly linear temperature gradient is present in the transverse direction of the laminate, disturbed by the initial crack only at the center of the laminate. Later the insulation provided by the crack becomes more significant and spreads with the growing crack.

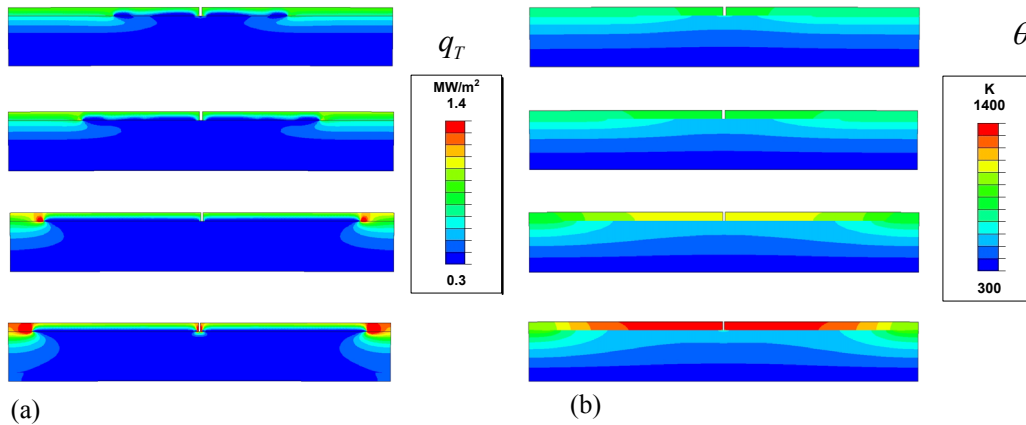


Figure 1 Contours of (a) predicted transverse heat flux at 4.75 s, 5 s, 6 s and 7 s; and (b) corresponding contour plots of the temperature distribution.

Finally, after the crack has extended significantly the temperature distribution is such that the protective coating is strongly heated through its entire thickness. The C-C laminate remains at significantly lower temperatures due to the insulation provided by the crack.

The conditions pertaining to the crack environment as well as the temperature dependence of the cohesive strength impact the crack growth behavior. Figure 2 depicts the predicted crack length as a function of time for constant and temperature dependent cohesive strength, and considers both loading in vacuum and a gas containing environment. Under vacuum conditions crack initiation occurs earlier than in an air-containing environment. However, the presence of the gas has less effect on the subsequent crack growth. As material separation progresses the material separation increases and makes the gas in the crack a less effective conductor. Computations accounting for the temperature dependence of the cohesive strength predict higher crack growth rates both for the vacuum and the gas case. As the specimen temperature increases material separation becomes easier.

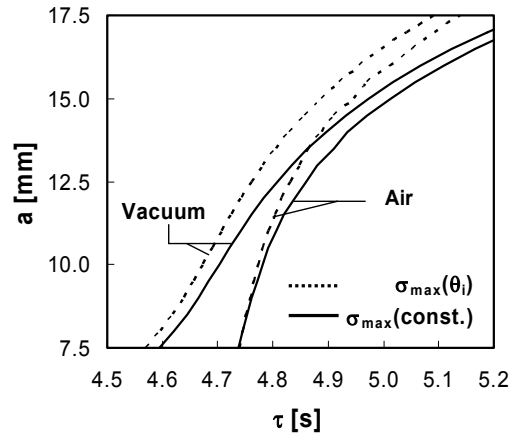


Figure 2 Predicted crack growth in the presence of air and under vacuum for temperature dependent and temperature independent cohesive strength.

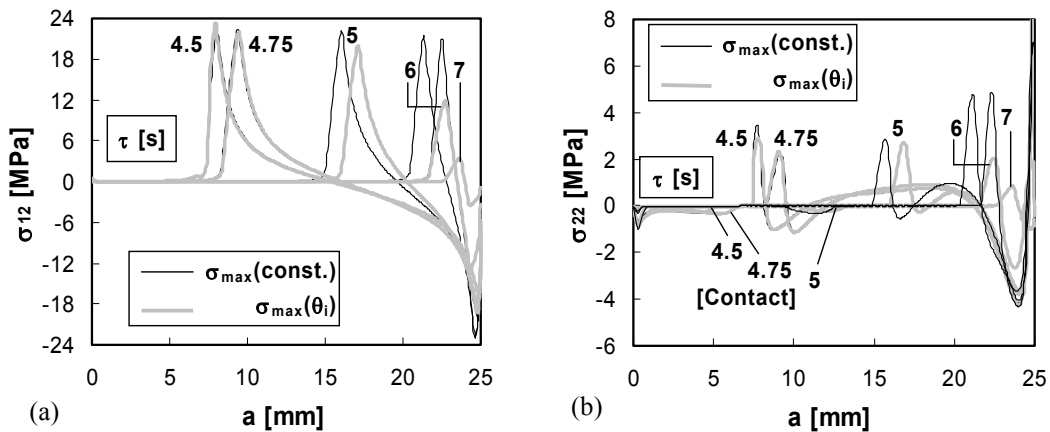


Figure 3 Predicted stress distributions along the interface (a) shear and (b) normal stresses.

An understanding of the crack propagation process can be obtained by investigating the stress state in the elements located adjacent to the interface, Figure 3. The failure process is dominated by shear. The computed stress distribution is crack like with the maximum value of shear stress at the location of the current crack tip. The values of normal stresses remain small, with a maximum near the current crack tip. In simulations with temperature independent cohesive strength, the peak values of stress are nearly constant throughout. If the temperature dependence of the cohesive strength is accounted for both the peaks in shear and normal stress decrease at later times as the temperature at the interface increases.

## 5 CONCLUSIONS

A numerical simulation approach is established to investigate crack propagation driven by an applied heat flux. Within the thermo-mechanical cohesive zone model coupling between the mechanical and thermal part occurs through the temperature dependent cohesive zone strength, the damage dependent interface conductance, the material separation dependent crack conductance and the contact conductance. The results of simulations of interface crack growth in a thermal protection system are presented.

## 6 ACKNOWLEDGEMENTS

The financial support from Sandia National Laboratories through the NSF-Sandia Life Cycle Engineering Program is gratefully acknowledged.

## 7 REFERENCES

- [1] Florence, A.L. and Goodier, J.N., *J. Appl. Mech.* 26, 293-294, (1959)
- [2] Kokini, K. and Reynolds, R.R., *J. Therm. Stresses* 15, 355-377, (1992)
- [3] Chao, C.K. and Chang, R.C., *J. Therm. Stresses* 17, 285-299, (1994)
- [4] Lee, K.Y. and Park, S.J., *Eng. Fract. Mech.* 50, 475-482, (1995)
- [5] Kokini, K. and Reynolds, R.R., *Eng. Fract. Mech.* 38, 371-383, (1991)
- [6] Lee, Y.D. and Erdogan, F., 1998. *Eng. Fract. Mech.* 59, 361-380, (1998)
- [7] Hutchinson, J.W., and Evans, A.G., *Surf. Coat. Tech.* 149, 179-184, (2002)
- [8] Kuo, A.Y., *J. Appl. Mech.* 57, 354-358, (1990)
- [9] Hutchinson, J.W. and Lu, T.J., *J. Eng. Mater. Tech.* 117, 386-390 (1995)
- [10] Elliot, H.A., *Proc. Phy. Soc. London* 59, 208, (1947)
- [11] Barenblatt, G.I., *Adv. Appl. Mech.* 7, 55-129, (1962)
- [12] Needleman, A., *J. Appl. Mech.* 54, 525-531 (1987)
- [13] Geubelle, P.H. and Baylor, J.S., *Composites Part B* 29, 589-602 (1998)
- [14] Zavarise, G., Wriggers, P., Stein, E., Schrefler, B.A., *Mech. Res. Comm.* 19, 173-182, (1992)
- [15] Liang, Y. and Sofronis, P., 2003. *J. Mech. Phy. Solids* 51, 1509-1531, (2003)
- [16] He, W.J. and Shioya, T., 1997. *Composites Part A* 28A, 689-694, (1997)
- [17] Columbia accident investigation board reports, [www.caib.org](http://www.caib.org), (2003)
- [18] Hattiangadi, A. and Siegmund, T., *J. Mech. Phy. Solids* 52, 533-566, (2004)
- [19] Mikic, B.B., *Int. J. Heat Mass Transfer* 17, 205-214, (1974)